

The 6dF Galaxy Survey: Final Redshift Release (DR3) and Southern Large-Scale Structures

D. Heath Jones¹, Mike A. Read², Will Saunders¹, Matthew Colless¹, Tom Jarrett³, Quentin A. Parker^{1,4}, Anthony P. Fairall^{5,15}, Thomas Mauch⁶, Elaine M. Sadler⁷, Fred G. Watson¹, Donna Burton¹, Lachlan A. Campbell^{1,8}, Paul Cass¹, Scott M. Croom⁷, John Dawe^{1,15}, Kristin Fiegert¹, Leela Frankcombe⁸, Malcolm Hartley¹, John Huchra⁹, Dionne James¹, Emma Kirby⁸, Ofer Lahav¹⁰, John Lucey¹¹, Gary A. Mamon^{12,13}, Lesa Moore⁷, Bruce A. Peterson⁸, Sayuri Prior⁸, Dominique Proust¹³, Ken Russell¹, Vicky Safouris⁸, Ken-ichi Wakamatsu¹⁴, Eduard Westra⁸, and Mary Williams⁸

¹Anglo-Australian Observatory, P.O. Box 296, Epping, NSW 1710, Australia (heath@aao.gov.au)

²Institute for Astronomy, Royal Observatory, Blackford Hill, Edinburgh, EH9 3HJ, United Kingdom

³Infrared Processing and Analysis Center, California Institute of Technology, Mail Code 100-22, Pasadena, CA 91125, USA

⁴Department of Physics, Macquarie University, Sydney 2109, Australia

⁵Department of Astronomy, University of Cape Town, Private Bag, Rondebosch 7700, South Africa

⁶Astrophysics, Department of Physics, University of Oxford, Keble Road, Oxford, OX1 3RH, UK

⁷School of Physics, University of Sydney, NSW 2006, Australia

⁸Research School of Astronomy & Astrophysics, The Australian National University, Weston Creek, ACT 2611, Australia

⁹Harvard-Smithsonian Center for Astrophysics, 60 Garden St MS20, Cambridge, MA 02138-1516, USA

¹⁰Department of Physics and Astronomy, University College London, Gower St, London WC1E 6BT, UK

¹¹Department of Physics, University of Durham, South Road, Durham DH1 3LE, United Kingdom

¹²Institut d'Astrophysique de Paris (CNRS UMR 7095), 98 bis Bd Arago, F-75014 Paris, France

¹³GEPI (CNRS UMR 8111), Observatoire de Paris, F-92195 Meudon, France

¹⁴Faculty of Engineering, Gifu University, Gifu 501-1193, Japan

¹⁵deceased.

Accepted —. Received —; in original form —.

ABSTRACT

We report the final redshift release of the 6dF Galaxy Survey, a combined redshift and peculiar velocity survey over the southern sky ($|b| > 10^\circ$). Its 136 304 spectra have yielded 110 256 new extragalactic redshifts and a new catalogue of 125 071 galaxies making near-complete samples with $(K, H, J, r_F, b_J) \leq (12.65, 12.95, 13.75, 15.60, 16.75)$. The median redshift of the survey is 0.053. Survey data, including images, spectra, photometry and redshifts, are available through an online database. We describe changes to the information in the database since earlier interim data releases. Future releases will include velocity dispersions, distances and peculiar velocities for the brightest early-type galaxies, comprising about 10% of the sample. Here we provide redshift maps of the southern local universe with $z \leq 0.1$, showing nearby large-scale structures in hitherto unseen detail. A number of regions known previously to have a paucity of galaxies are confirmed as significantly underdense regions. The URL of the 6dFGS database is <http://www-wfau.roe.ac.uk/6dFGS>.

Key words: surveys — galaxies: clustering — galaxies: distances and redshifts — cosmology: observations — cosmology: large scale structure of universe

1 INTRODUCTION

The advent of wide-field multiplexing spectrographs over the past decade has produced huge advances in our

Table 1. Comparison of recent wide-area low-redshift galaxy surveys

	6dFGS	2dFGRS	SDSS-DR7
Magnitude limits	$K \leq 12.65$ $H \leq 12.95$ $J \leq 13.75$ $r_F \leq 15.60$ $b_J \leq 16.75$	$b_J \leq 19.45$	$r \leq 17.77$ (Petrosian)
Sky coverage (sr)	5.2	0.5	2.86
Fraction of sky	41%	4%	23%
Extragalactic sample, N	125 071	221 414	644 951
Median redshift, $z_{\frac{1}{2}}$	0.053	0.11	0.1
Volume V in $[0.5z_{\frac{1}{2}}, 1.5z_{\frac{1}{2}}]$ ($h^{-3} \text{Mpc}^3$)	2.1×10^7	1.7×10^7	7.6×10^7
Sampling density at $z_{\frac{1}{2}}$, $\bar{\rho} = \frac{2N}{3V}$ ($h^3 \text{Mpc}^{-3}$)	4×10^{-3}	9×10^{-3}	6×10^{-3}
Fibre aperture ($''$)	6.7	2.0	3.0
Fibre aperture at $z_{\frac{1}{2}}$ ($h^{-1} \text{kpc}$)	4.8	2.8	3.9
Reference(s)	(1)	(2)	(3)

Taking $h = H_0/100 \text{ km s}^{-1} \text{ Mpc}^{-1}$, $\Omega_{M_0} = 0.3$, and $\Omega_{\Lambda_0} = 0.7$. References: (1) this paper; (2) Colless et al. (2001), Cole et al. (2005); (3) Abazajian et al. (2009), www.sdss.org/dr7, (`PetroMag_r < 17.77`, `type = 3`, `zStatus > 2`, and objects with stellar morphology and $z > 0.001$).

knowledge of the structure and content of the low-redshift universe. Surveys such as the 2dF Galaxy Redshift Survey (2dFGRS; Colless et al. 2001) and the Sloan Digital Sky Survey (SDSS; York et al. 2000; Abazajian et al. 2009) have characterised the luminosity and clustering properties of galaxies in unprecedented detail and measured with unprecedented precision the amount and spatial distribution of dark matter. They also place tight constraints on Λ -Cold Dark Matter models of the universe (e.g. Spergel et al. 2007) when combined with the results of supernovae distance measurements (Schmidt et al. 1998; Riess et al. 1998; Perlmutter et al. 1999) and the cosmic microwave background (Bennett et al. 2003). Within this context, the focus has shifted towards an improved understanding of galaxy mass assembly and structure formation generally (e.g. Baugh 2006). A combined redshift and peculiar velocity survey, with dynamical measures of galaxy masses and large-scale motions, offers even better constraints on parameters of cosmological interest than a survey of redshifts alone (Burkey & Taylor 2004; Zaroubi & Branchini 2005).

The 6dF Galaxy Survey¹ (6dFGS; Jones et al. 2004, 2005) is a near-infrared-selected redshift and peculiar velocity survey that is complete to total extrapolated magnitude limits $(K, H, J) = (12.65, 12.95, 13.75)^2$ over

¹ 6dFGS home: <http://www.aao.gov.au/6dFGS>

² These limits differ slightly from those reported in Jones et al. (2004) and Jones et al. (2005) due to subsequent revision of the input magnitudes by 2MASS and SuperCOSMOS; see Sec. 2.

83 percent of the southern sky. The near-infrared total JHK magnitudes are taken from the Two Micron All-Sky Survey (2MASS) Extended Source Catalog (XSC; Jarrett et al. 2000), while $b_J r_F$ photometry comes from SuperCOSMOS (Hambly et al. 2001a,b), following its recalibration for the 2dF Galaxy Redshift Survey (Cole et al. 2005).

Near-infrared (NIR) selection of the primary galaxy samples is advantageous because it closely tracks the older stellar populations that dominate the stellar mass in galaxies. Furthermore, extinction (both internal and Galactic) is greatly lessened and stellar mass-to-light ratios are more tightly defined (Bell & de Jong 2001). Two secondary optically-selected samples are complete to $(r_F, b_J) = (15.60, 16.75)^2$. A number of smaller samples, selected from various catalogues and wavelengths, fill out the target allocations. The peculiar velocity survey uses velocity dispersions and photometric scale-lengths to derive dynamical masses and Fundamental Plane distances and peculiar velocities for a subset of more than 10 000 bright, early-type galaxies.

The 6dFGS magnitude limits are ~ 1.5 mag brighter than the magnitudes at which incompleteness starts to affect the 2MASS XSC ($K \lesssim 14$). Examination of the bivariate distribution of surface brightness and galaxy luminosity for the entire 6dFGS sample (Jones et al., in prep) shows sample selection to be robust against surface brightness selection effects (see e.g. Bell et al. 2003; McIntosh et al. 2006). The limiting isophote at which 6dFGS magnitudes were measured ($\mu_K = 20 \text{ mag arcsec}^{-2}$) is brighter than the values at which 2MASS was found to be incomplete by these authors.

The 6dFGS has thus far been used in studies of large-scale structure (e.g. Fleenor et al. 2005, 2006; Boué et al. 2008; Radburn-Smith et al. 2006; Proust et al. 2006), luminosity and stellar mass functions (Jones et al. 2006, Jones et al., in prep), the influence of local density and velocity distributions (Erdogdu et al. 2006a,b), among others. The Early and First Data Releases (see below) alone yielded new redshifts for 277 ACO clusters ($z \lesssim 0.1$) without previous redshifts (Andernach et al. 2005), and the full data have yielded more than 400. Examples of the full 3-d space structure of the 6dFGS can be seen in Fluke, Barnes & Jones (2008). The 6dFGS has also been used to study special interest samples selected for their luminosity at x-ray and radio wavelengths (Sadler et al. 2007; Mauduit & Mamon 2007; Mauch & Sadler 2007). Future surveys with next generation radio telescopes such as ASKAP and the SKA (e.g. Blake et al. 2004; van Driel 2005; Rawlings 2006) will also benefit from the legacy of 6dFGS, as they probe comparable volumes in HI with the benefit of prior redshift information across most of the southern sky.

This paper describes the final data release of 6dFGS redshifts. Earlier incremental data releases in 2002 December, 2004 March and 2005 May have made the first 90k redshifts publicly available through an online database. In Sec. 2 we give an overview of the 6dF Galaxy Survey including the characteristics and scope of the data set. Section 3 describes the final instalment as well as its access through our online database. Details of changes

and additions superseding earlier releases are also given. In Sec. 4 we present redshift maps of the southern sky in both equatorial and Galactic coordinate projections, and discuss major large-scale structures. Concluding remarks are made in Sec. 5.

2 SURVEY OVERVIEW

2.1 Background

The primary references for detailed information about the 6dFGS are Jones et al. (2004) and this paper. The former describes target selection and field allocations, the 6dF instrument, and data reduction and redshifting methodology. It also characterises the First Data Release (DR1; 46k redshifts) and the online database. Jones et al. (2005) describes the Second Data Release (DR2; 83k redshifts) and discusses a number of small changes to the data. Earlier papers describe the 6dF instrument (Parker, Watson, & Miziarski 1998; Watson et al. 2000) and the field placement algorithm used to optimise target coverage (Campbell, Saunders, & Colless 2004). Database users are encouraged to consult these and other papers on the 6dFGS Publications web page³. This paper marks the final public data release of 6dFGS redshift data.

The observations for this survey were carried out using the Six Degree Field (6dF) fibre-fed multi-object spectrograph at the UK Schmidt Telescope (UKST) over 2001 May to 2006 January (Jones et al. 2004). Target fields covered the $\sim 17\,000$ deg² of southern sky more than 10° from the Galactic Plane⁴, approximately ten times the area of the 2dF Galaxy Redshift Survey (2dFGRS; Colless et al. 2001) and more than twice the spectroscopic areal coverage of the Sloan Digital Sky Survey seventh data release (SDSS DR7; Abazajian et al. 2009). Table 1 shows a comparison of the 6dFGS to these two major surveys. In terms of secure redshifts, 6dFGS has around half the number of 2dFGRS and one-sixth those of SDSS DR7 ($r < 17.77$). The co-moving volume covered of 6dFGS is about the same as 2dFGRS at their respective median redshifts, and around 30 percent that of SDSS DR7. In terms of fibre aperture size, the larger apertures of 6dFGS (6.7'') give a projected diameter of $4.8 h^{-1}$ kpc at the median redshift of the survey, covering 40 percent more projected area than SDSS at its median redshift, and more than three times the area of 2dFGRS. By any measure, the scale of 6dFGS is readily comparable to those of SDSS and 2dFGRS, and like those surveys, its legacy is a permanent public database, which is unique in its scope, depth and southern aspect.

Figure 1 shows the sky distribution of 6dFGS targets and fields. Of the 1 526 fields observed, 1 447 contributed data to the final survey. The remaining 5 percent were rejected for reasons of quality control. Of the 1 447, around half have completeness greater than 90 percent, and more

than two thirds have completeness greater than 85 percent. Although most sky regions are effectively covered twice, around 50 fields near the LMC and the South Pole were not observed by the conclusion of the survey. Sky redshift completeness (Fig. 1c) is generally high (85 percent or greater) but diminishes in regions with insufficient coverage or affected by poor conditions. In terms of survey limiting magnitude, m_{lim} , completeness is greater than 85 percent for $m < (m_{\text{lim}} - 0.75)$ in fields with completeness 90 percent or higher, and for $m < (m_{\text{lim}} - 2)$ in fields with completeness of 70 to 80 percent.

2.2 Redshift Distribution

The median redshift for 6dFGS is $z_{1/2} = 0.053$, roughly half that of SDSS and 2dFGRS, and twice that of the 2MASS Redshift Survey (2MRS; Erdoğdu et al. 2006a). Figure 2 shows the number distribution of 6dFGS redshifts for both the full sample, $N(z)$, (panel *b*; 125 071 sources) as well as the K -selected primary targets, $N_K(z)$, (panel *c*; 93 361). Both samples show the skewed distributions typical for magnitude-limited surveys, which is accentuated in Fig. 2(*b*) by the inclusion of Additional Target samples that stretch the overall distribution to higher redshifts. This is also reflected in their interquartile ranges: [0.034, 0.074] for the full sample, compared to the slightly narrower [0.034, 0.070] for the K -selected sample. The localised peaks in $N(z)$ and $N_K(z)$ are due to individual large-scale structures, clearly seen in Fig. 2(*a*) when redshifts are spread across RA. The gaps in (*a*) centred on R.A. 8 hr and 17 hr correspond to the unsurveyed regions around the Galactic Plane.

The limit of the K -selected sample ($K \leq 12.65$) encompasses galaxies with luminosities $M_K \leq -23.24$ at the median redshift ($z_{1/2} = 0.053$), around 0.6 mag fainter than M^* , the characteristic turn-over point in the K -band luminosity function from the same sample (Jones et al. 2006, Jones et al. in prep.). Integrating this luminosity function over the volume covered by 6dFGS in each redshift shell Δz yields the expected number-redshift distribution $N_{\text{LF}}(z)$. As the K -band luminosity function contains completeness corrections that the raw $N_K(z)$ distribution does not, the ratio

$$\frac{\int_0^\infty N_K(z) dz}{\int_0^\infty N_{\text{LF}}(z) dz} = 0.9245 \quad (1)$$

is slightly less than unity. The blue dashed curve representing $N_{\text{LF}}(z)$ in Fig. 2(*c*) has been scaled by this amount, and the ratio of the two distributions $N_K(z) / N_{\text{LF}}(z)$ gives the normalisation due to overall incompleteness. Any redshift differences between the curve and the data are due to magnitude-dependent incompleteness, which in turn imparts redshift differences in selection. Furthermore, a Schechter function is not a perfect fit to the luminosity function across all luminosities. The reader is referred to the 6dFGS luminosity function papers (Jones et al. 2006, Jones et al. in prep.) for a more detailed discussion of survey selection functions.

The curve $N_{\text{LF}}(z)$ (uncorrected for incompleteness) is well-fit by the empirical function

$$N_{\text{fit}}(z) = A z^\gamma \exp[-(z/z_p)^\gamma] \quad (2)$$

³ <http://www.aao.gov.au/6dFGS/Publications>

⁴ The b_J and r_F surveys of 6dFGS are limited to $|b| > 20^\circ$ in order to mitigate the effect of higher Galactic extinction in the optical at lower latitudes.

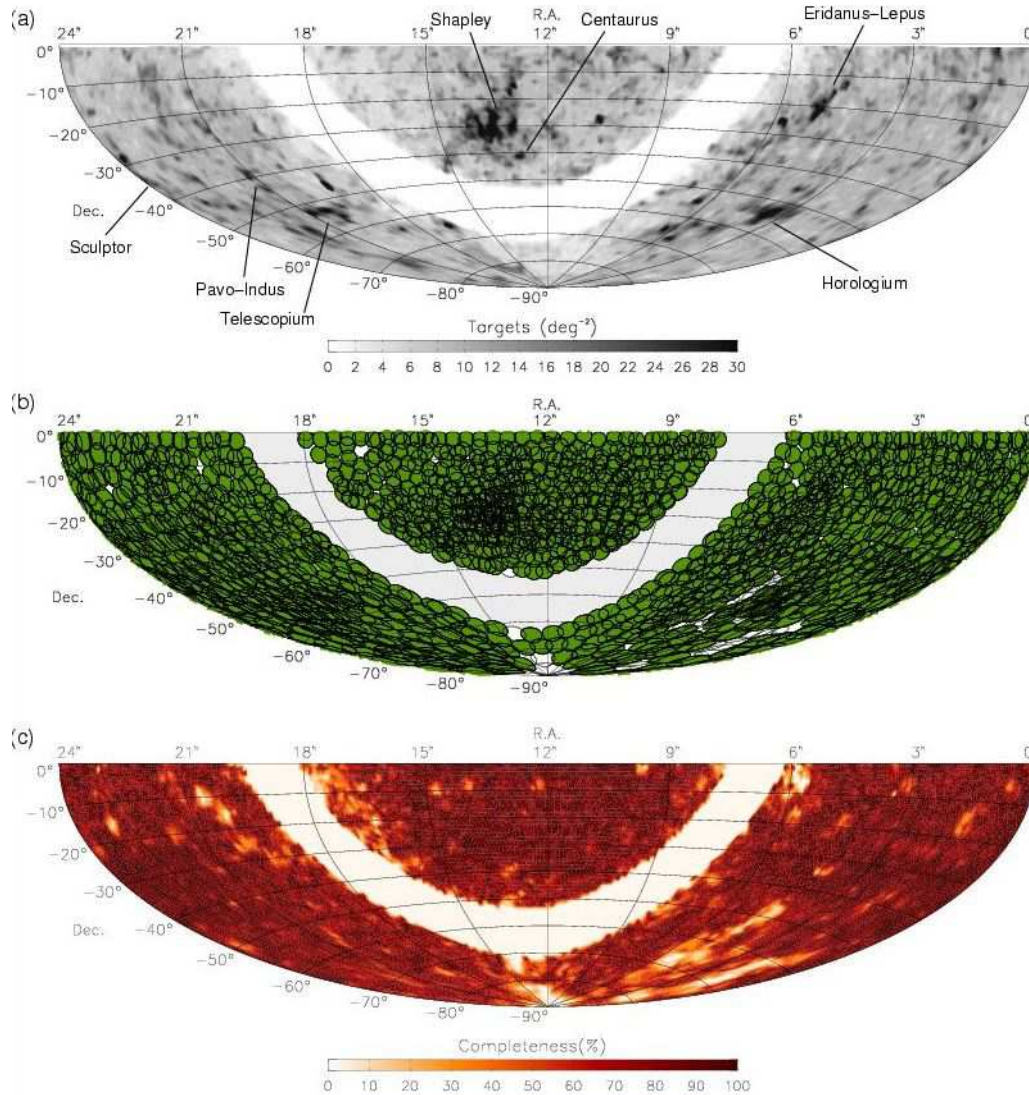


Figure 1. (a) Density of 6dFGS target sources (per square degree) on the sky; key supercluster over-densities are labelled. (b) Full 6dFGS field coverage (filled discs) and unobserved target fields (open circles). (c) Redshift completeness for $K \leq 12.65$. All panels show equal-area Aitoff projections.

with values $\gamma = 1.6154 \pm 0.0001$, $z_p = 0.0446 \pm 0.0001$, and $A = 622978 \pm 10$ (Fig. 2c; red solid line, also scaled by 0.9245). This 3-parameter function is a simpler variant of the 4-parameter fits used by Erdogdu et al. (2006a) and Colless et al. (2001) for the 2MRS and 2dFGRS samples, respectively, but fits the 6dFGS K -band sample well. In this case, the value of z_p locates the peak in the distribution, which is slightly lower than the median of the data, and corresponds to a limiting absolute magnitude of $M_K = -22.97$ (~ 1 mag fainter than M^*). Even so, the remarkable consistency between the K -band luminosity function distribution ($N_{LF}(z)$) and that of the data ($N_K(z)$) underscores the homogeneity of the primary sample.

2.3 Sample Composition

The original target catalogue for 6dFGS contained 179 262 sources, one third of which originated from out-

side the near-infrared selected catalogues. Around 8 percent of these sources had existing redshifts from ZCAT (9 042; Huchra et al. 1992), the 2dF Galaxy Redshift Survey (5 210; Colless et al. 2001), or the Sloan Digital Sky Survey DR7 (563; Abazajian et al. 2009). 6dFGS spectra were obtained in 136 304 source observations and yielded 126 754 unique redshifts of varying quality.

6dFGS redshift quality, Q , was classified on a scale of 1 to 6 through visual assessment of every redshift, with $Q = 1$ assigned to unusable measurements, $Q = 2$ to possible but unlikely redshifts, $Q = 3$ for reliable redshifts and $Q = 4$ for high-quality redshifts. Stars and other confirmed Galactic sources are assigned $Q = 6$ (there is no $Q = 5$). Some legitimate QSO redshifts classified earlier in the survey carry $Q = 2$ because no QSO-specific templates were employed to classify QSO redshifts until midway through the survey. Unlike SDSS, no lower velocity limit has been used to discriminate between Galactic and extragalactic sources; assignment of $Q = 6$ is on the basis

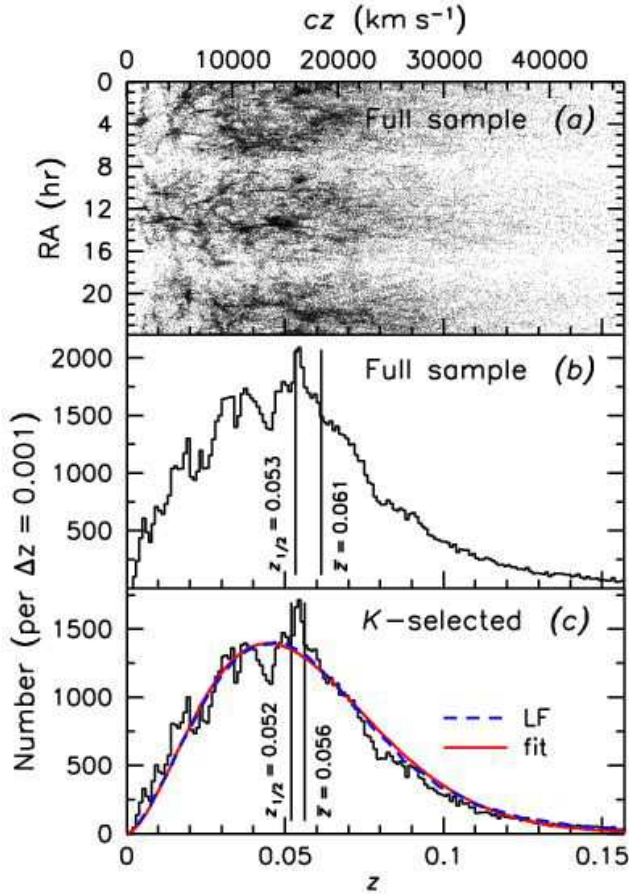


Figure 2. Distribution of all 6dFGS redshifts in terms of (a) right ascension and (b) number. Panel (c) shows the same as (b) but limited to the primary K -selected sample. The dashed blue line is the redshift distribution calculated from the K -band luminosity function of the same sample (Jones et al., in prep). The solid red line is an empirical fit to the blue curve.

of spectral appearance as well as recession velocity. Cases of overlap between galaxies and foreground stars evident from imaging data were re-examined, and are discussed in Sec. 3. Table 2 gives the breakdown of these numbers across individual 6dFGS sub-samples.

Only $Q = 3, 4$ redshifts should be used in any galaxy analysis. (The distinction between $Q = 3$ and $Q = 4$ is less important than that between $Q = 2$ and $Q = 3$, since the former represent a successful redshift in either case.) Galaxies with repeat observations have all spectra retained in the database, and the final catalogued redshift is a weighted mean of the measurements with $Q = 3, 4$, excluding redshift blunders. Descriptions of the redshift quality scheme in its previous forms can be found in Sec. 2.1 of Jones et al. (2005) and Sec. 4.4 of Jones et al. (2004).

Unreliable ($Q = 2$) or unusable ($Q = 1$) galaxy redshifts together comprise around 8 percent of the redshift sample. Galactic sources ($Q = 6$) represent another 4 percent. The remaining 110 256 sources with $Q = 3, 4$ are the robust extragalactic 6dFGS redshifts that should be used

Table 2. Breakdown of 6dFGS and literature redshifts.

6dFGS by Q value:	
$Q = 1$, unusable data	5 787 (4.6 pc)
$Q = 2$, unlikely redshifts	5 592 (4.4 pc)
$Q = 3$, reliable redshifts	8 173 (6.4 pc)
$Q = 4$, high quality redshifts	102 083 (80.5 pc)
$Q = 6$, Galactic sources	5 119 (4.0 pc)
Total	126 754 (100 pc)
Literature redshifts:	
SDSS	563 (3.8 pc)
2dFGRS	5 210 (35.2 pc)
ZCAT	9 042 (61.0 pc)
Total	14 815 (100 pc)

References: SDSS: Abazajian et al. (2009), 2dFGRS: Colless et al. (2001), ZCAT: Huchra et al. (1992)

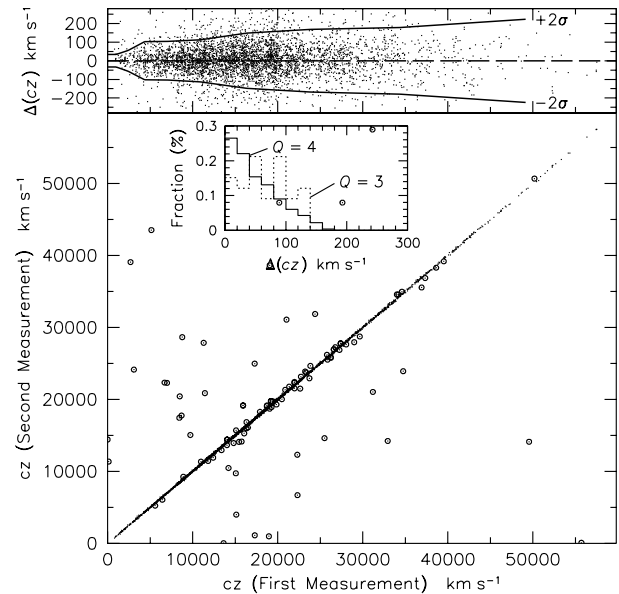


Figure 3. (Top panel:) Repeat 6dF redshift measurements for a sample of 6dFGS galaxies obtained with the VPH gratings over the period 2002.5 to 2006 (4570 galaxies). Redshift blunders (circled) are those for which $|\Delta cz| > 330 \text{ km s}^{-1}$. (Inset panel:) Distribution of the $|\Delta cz|$ differences for the individual redshift quality $Q = 3$ (dotted line) and $Q = 4$ (solid line) samples, normalised to the total sample size in each case. (Bottom panel:) Distribution of redshift difference as a function of redshift, with a running $\pm 2\sigma$ boundary (solid lines).

(alongside the 14 815 literature redshifts) in any analysis or other application. Tables 2 and 3 give the breakdown of these numbers across various 6dFGS sub-samples.

2.4 Redshift uncertainties and blunder rates

Redshift uncertainties and blunder rates were estimated from the sample of 6dFGS galaxies with repeat red-

Table 3. Final numbers of spectra and redshifts in the 6dFGS samples.

ID	Survey sample	6dFGS spectra	Good z	Lit. z	Total z
1	2MASS $K_s \leq 12.75$	97 020	83 995	9 340	93 335
3	2MASS $H \leq 12.95$	2 021	1 742	255	1 997
4	2MASS $J \leq 13.75$	1 284	1 096	175	1 271
5	DENIS $J \leq 14.00$	629	488	115	603
6	DENIS $I \leq 14.85$	504	234	109	343
7	SuperCOS $r_F < 15.6$	5 773	5 025	1 221	6 246
8	SuperCOS $b_J < 16.75$	6 516	5 885	1 236	7 121
78	Dur./UKST extension	271	207	30	237
90	Shapley supercluster	630	494	40	534
109	Horologium sample	469	384	41	425
113	ROSAT all-sky survey	1 961	1 126	190	1 316
116	2MASS Red AGN	1 141	438	140	578
119	HIPASS ($> 4\sigma$)	439	354	116	470
125	SUMSS/NVSS radio	2 978	1 351	272	1 623
126	IRAS FSC ($> 6\sigma$)	5 994	4 208	1 239	5 447
129	Hamburg-ESO QSOs	2 006	624	123	747
130	NRAO-VLA QSOs	2 673	293	41	334
≥ 999	unassigned targets [†]	3 995	2 312	132	2 444
	Total	136 304	110 256	14 815	125 071

[†] Objects removed from the initial target list (due to changes in the 2MASS source catalogue after 6dFGS was underway). ID = 999 or 9999 in these cases.

Columns:

- (1) ID: Programme ID (PROGID in the database; see Sec. 3).
- (2) Survey sample: first sample (in order of PROGID) in which object is found.
- (3) 6dFGS spectra: number of spectra obtained for this sample.
Note that some objects were observed more than once. The numbers include spectra of all qualities and Galactic sources.
- (4) Good z : number of robust extragalactic 6dFGS redshifts, (those with $Q = 3$ or 4). Reflects contents of database.
- (5) Lit. z : additional literature extragalactic redshifts (ignoring repeats and overlaps).
- (6) Total z : total number of extragalactic redshifts for objects in this sample.

shift measurements. There were 8 028 such redshift pairs, 43 percent of which were first-year (pre-2002.5) data. Most repeat measurements were made because of a low-quality initial measurement, or because of a change in the field tiling strategy after the first year of observations. We define a blunder as a redshift mismatch of more than 330 km s^{-1} (5σ) between a pair of redshift measurements that we would expect to agree. The blunder rate on individual 6dFGS redshifts is 1.6 percent, the same as reported for the First Data Release (Jones et al. 2004). In late 2002, a new transmissive Volume-Phase Holographic (VPH) gratings (580V and 425R) replaced the existing reflection gratings (600V and 316R), resulting in improved throughput, uniformity, and data quality. Excluding first-year repeats reduces the individual blunder

rate to 1.2 percent. While the first-year data represent nearly half of all repeat measurements, they represent less than a fifth of the overall survey. Table 4 summarises the blunder rates and other statistics for both the full and post-first-year data.

Figure 3 shows repeat redshift measurements for 6dFGS observations with the VPH gratings, representative of the great majority of survey spectra (around 80 percent: 4 570 sources spanning 2002.5 to 2006). Blunder measurements (106 of them) have been circled, and the scatter in redshift offset, Δcz , as a function of redshift is also shown. Not surprisingly, redshifts becoming increasingly difficult to secure as one moves to higher values. The inset in Figure 3 displays the distribution in $|\Delta cz|$ for measurement pairs grouped by their redshift quality $Q = 3$ or 4 classifications. There are 3 611 pairs in the non-blunder sample with both measurements of quality $Q = 4$, with scatter implying a redshift uncertainty in an individual $Q = 4$ measurement of $\Delta cz(4) = 46 \text{ km s}^{-1}$. Likewise, the scatter in the much smaller $Q = 3$ sample (33 pairs) suggests $\Delta cz(3) = 55 \text{ km s}^{-1}$. If we include the pre-2002.5 non-VPH data, the implied redshift uncertainties are unchanged for $Q = 4$ and increase slightly in the case of $Q = 3$ ($\Delta cz(3) = 67 \text{ km s}^{-1}$). Note that these redshift uncertainties are less than those estimated in Jones et al. (2004) from the First Data Release, demonstrating the improved integrity of the 6dFGS data since the early releases.

An external comparison of 6dFGS redshifts to those overlapping the Seventh Data Release (DR7) of the Sloan Digital Sky Survey (SDSS; Abazajian et al. 2009) was also made and is shown in Fig. 4. Although the full SDSS DR7 contains over a million classified extragalactic spectra, almost all are too northerly to overlap significantly with the southern 6dFGS or are too faint. However, the 2 459 sources in common to both catalogues provide a valuable test of redshift success rates. The pair-wise blunder fraction in this case is 3.9 percent. Splitting this with the 6dFGS blunder rate of 1.2 percent implies an SDSS blunder rate of 2.7 percent, although the 6dFGS blunder rate at the fainter SDSS magnitudes is likely to be somewhat higher than the 1.2 percent measured overall.

3 NEW DATA RELEASE

3.1 Online database

The 6dFGS Online Database is hosted at the Wide Field Astronomy Unit of the Institute for Astronomy⁵ at the University of Edinburgh. Data are grouped into 15 inter-linked tables consisting of the master target list, all input catalogues, and their photometry. Users can obtain FITS and JPEG files of 6dFGS spectra as well as 2MASS and SuperCOSMOS postage stamp images in JHK and $b_J r_F$ where available, and a plethora of tabulated values for observational quantities and derived photometric and spectroscopic properties. The database can be queried in either its native Structured Query Language

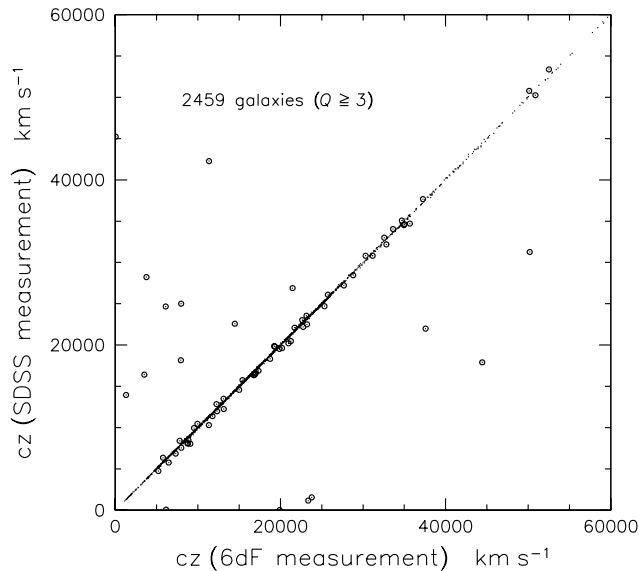
⁵ <http://www-wfau.roe.ac.uk/6dFGS>

Table 4. Redshift uncertainties and blunder rates from both internal and external comparisons of 6dFGS.

6dFGS (full sample):	
Total repeat measurements ($Q \geq 3$):	8028
RMS scatter of all redshift measurement pairs [†]	66 km s ⁻¹
$Q = 4$ redshift uncertainty (6051 sources)	45 km s ⁻¹
$Q = 3$ redshift uncertainty (104 sources)	67 km s ⁻¹
Number of blunders [‡] ($Q \geq 3$):	260
6dFGS pair-wise blunder rate:	3.2%
6dFGS single-measurement blunder rate:	1.6%
6dFGS (VPH grating only, 2002.5 – 2006):	
Total repeat measurements ($Q \geq 3$):	4570
RMS scatter of all redshift measurement pairs [†]	67 km s ⁻¹
$Q = 4$ redshift uncertainty (3611 sources)	46 km s ⁻¹
$Q = 3$ redshift uncertainty (33 sources)	55 km s ⁻¹
Number of blunders [‡] ($Q \geq 3$):	106
6dFGS pair-wise blunder rate:	2.3%
6dFGS single-measurement blunder rate:	1.2%
6dFGS (VPH only) vs. SDSS DR7:	
Number of comparison sources ($Q \geq 3$):	2459
Number of blunders [†] ($Q \geq 3$):	95
Pair-wise blunder rate:	3.9%
Implied blunder rate for SDSS:	2.7%

[†] Clipping the most extreme 10% of outliers (5% either side).

[‡] A blunder is defined as having $\Delta cz > 330 \text{ km s}^{-1} (5\sigma)$.

**Figure 4.** Redshift comparison of 6dFGS (VPH grating) with SDSS Data Release 7 (Abazajian et al. 2009).

(SQL) or via an HTML web-form interface. More complete descriptions are given elsewhere (Jones et al. 2004, 2005), although several new aspects of the database are discussed below. Figure 5 shows two examples of the way data are presented in the database.

Table 5 shows the full parameter listing for the 6dFGS database. Individual database parameters are grouped into lists of related data called *tables*. Parameter definitions are given in documentation on the database web site. The **TARGET** table contains the original target list for 6dFGS, and so contains both observed and unobserved objects. Individual entries in this table are celestial sources, and the **TARGETID** parameters are their unique integer identifiers. Note that the original target list *cannot* be used to estimate completeness, due to magnitude revisions in both the 2MASS XSC and SuperCOSMOS magnitudes subsequent to its compilation. Item (iv) below discusses this important issue in more detail.

The **SPECTRA** table holds the redshift and other spectroscopic data obtained by the 6dF instrument through the course of the 6dFGS. Many new parameters have been introduced to this table for this release (indicated in Table 5 by the † symbol). Individual entries in this table are spectroscopic observations, meaning that there can be multiple entries for a given object. The **SPECID** parameter is the unique integer identifier for 6dFGS observations.

Most 6dFGS spectra consist of two halves, observed separately through different gratings, and subsequently spliced together: a V portion ($\lambda\lambda 3900\text{--}5600\text{\AA}$) and an R portion ($\lambda\lambda 5400\text{--}7500\text{\AA}$).⁶ (Data taken prior to October 2002 used different gratings, spanning $4000\text{--}5600\text{\AA}$ and $5500\text{--}8400\text{\AA}$.) Various parameters in **SPECTRA** belonging to the individual V or R observations carry a *_V* or *_R* suffix, and are listed in Table 5 for V (with slanted font to indicate that there is a matching set of R parameters).

The **TWOMASS** and **SUPERCOS** tables hold relevant 2MASS XSC and SuperCOSMOS photometric and spatial information. Likewise, the remaining eleven tables contain related observables from the input lists contributing additional 6dFGS targets to **TARGET**. While some of the parameter names have been duplicated between tables (e.g. **MAG_1**, **MAG_2**) their meaning changes from one table to the next, as indicated in Table 5.

Database tables can be queried individually or in pairs. Alternatively, positional cross-matching (R.A. and Dec.) can be done between database sources and those in a user-supplied list uploaded to the site. Search results can be returned as HTML-formatted tables, with each entry linking to individual GIF frames showing the 6dFGS spectrum alongside its $b_J r_F JHK$ postage stamp images, as shown in Fig. 5. Individual object FITS files of the same data can also be accessed in this way. Long database returns can also be emailed to the user as an ASCII comma-separated variable (CSV) text file. Alternatively, the FITS files of all objects found through a search can be emailed to the user as a single tar file under a *TAR saveset* option.

Additional downloads in the form of ASCII files are also available from the database web site. These include

⁶ V and R here are not related to standard V or R passbands.

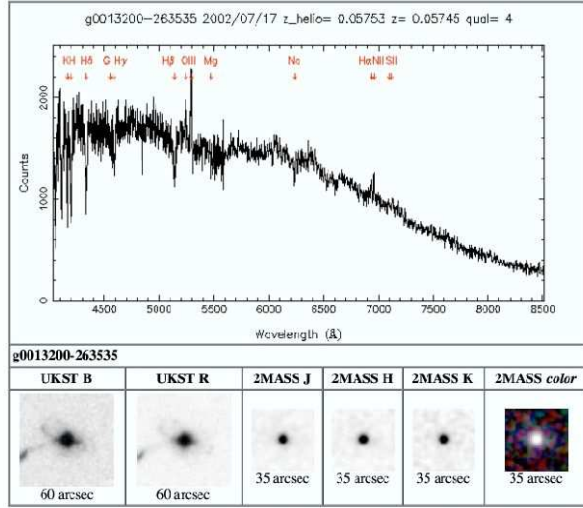
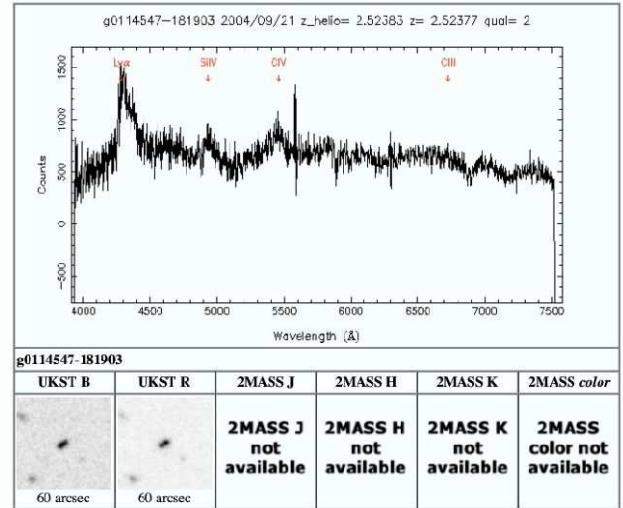
(a) Displaying spectrum with `specid=2632` and thumbnails for associated target `g0013200-263535`[Link to object's FITS file](#)(b) Displaying spectrum with `specid=8750` and thumbnails for associated target `g0114547-181903`[Link to object's FITS file](#)

Figure 5. Example spectroscopic and photometric frames from the 6dFGS online database for (a) a nearby bright galaxy at $z = 0.057$ ($Q = 4$) from the K -selected sample ($\text{PROGID} = 1$), and (b) a candidate double QSO at $z = 2.524$ ($Q = 2$) from the Hamburg-ESO QSO sample ($\text{PROGID} = 129$). 2MASS and UKST frames are only available for sources selected as part of the original 6dFGS primary samples, where available in one or more of $KHJr_{FBJ}$.

a master catalogue compilation of all redshifts (from both 6dFGS and the literature), as well as a comma-separated file of the spectral observations. The latter contains an entry for every 6dFGS observation held by the database (including repeats), regardless of redshift quality. The master catalogue attempts to assign the best available redshift to those sources determined to be extragalactic. In the case of repeats, a combined 6dFGS redshift is obtained by error-weighting ($1/(\Delta cz)^2$) those $Q = 3, 4$ redshifts within 5σ (330 km s^{-1}) of an initial $Q = 3, 4$ median, thereby excluding blunders. Where literature redshifts exist and are consistent with the 6dFGS redshift, the latter is used in the catalogue. In cases of disagreement ($> 5\sigma$ difference), the 6dFGS redshift is taken and the mismatch is flagged. Literature redshifts are use, where they exist, for objects that 6dFGS failed to secure. The master catalogue includes the `TARGETID` for each object and the `SPECID` references for each 6dFGS observation contributing to the final redshift, to facilitate cross-referencing with the 6dFGS database. Completeness maps (calculated from the revised target lists, after 2MASS and SuperCOS magnitude changes) will be made available at a future date.

Table 6 lists a subset of the more commonly-used database parameters, along with detailed descriptions. New parameters for this final release are indicated. Users should pay particular attention to the important differences between parameters which have similar-sounding names but which are significantly different in purpose. Examples to note are: (i) `Z`, `Z_ORIGIN`, `Z_HELIO`, `Z_INITIAL`, and `Z_HELIO_INITIAL`, (ii) `QUALITY` and `Q_FINAL`, (iii) (`JTOT`, `HTOT`, `KTOT`), (`J`, `H`, `K`), and (`MAG1`, `MAG2`) (from the `TWOMASS` table), and, (iv) (`BMAG`, `RMAG`),

(`BMAGSEL`, `RMAGSEL`) and (`BMAG`, `RMAG`) (from the `SUPERCOS` table). Table 6 details the differences between them.

3.2 Changes made for the final redshift release

All of the changes previously implemented for DR2 (Jones et al. 2005) have been retained, with some modifications. In particular, some fields rejected from earlier data releases on technical grounds have been fixed and included in the final release. The final data span observations from 2001 May to 2006 January inclusive. New changes are as follows:

(i) **Revised 2MASS Names:** Between the creation of the initial 6dFGS target list in 2001 and the final 2MASS XSC data release in 2004, the 2MASS source designations changed in the last two digits in both the R.A. and Dec. components of the source name. The original 2MASS names (previously held in the 6dFGS database `TWOMASS` table under the attribute `CATNAME`) have been retained but re-badged under a new attribute `PREVCATNAME`. The revised 2MASS names are stored in `CATNAME` and are consistent with the final data release of the 2MASS XSC. Original 6dFGS sources that were subsequently omitted from the final 2MASS data release have `CATNAME = ''`.

(ii) **Revised 2MASS Photometry:** The JHK total magnitudes used to select 6dFGS sources were also revised by 2MASS between 2001 and 2004. These new values are held in the newly-created `JTOT`, `HTOT`, `KTOT`. The revisions amount to less than 0.03 mag, except in the case of corrected blunders. The old magnitudes used for target selection continue to be held in `J`, `H` and `KEXT_K`, the latter being derived from surface brightness-corrected 2MASS extrapolated magnitudes (see Jones et al. (2004) for a full discussion).

Table 5. Full parameter listing for all tables in the 6dFGS database.

Table name	Description	PROGID	Parameters
TARGET	the master target list	–	TARGETID, TARGETNAME, HTMID, RA, DEC, CX, CY, CZ, GL, GB, A_V, PROGID, BMAG, RMAG, SG, ZCATVEL, ZCATERR, ZCATREF, BMAGSEL, RMAGSEL, TEMPLATECODE†, FRAMENAME
SPECTRA	redshifts and observational data	–	SPECID, TARGETID, TARGETNAME, OBSRA, OBSDEC, MATCH_DR, HTMID, CX, CY, CZ, Z_ORIGIN, Z, Z_HELIO, QUALITY, ABEMMA, NMBEST, NGOOD, Z_EMI, Q_Z_EMI, KBESTR, R_CRCOR, Z_ABS, Q_Z_ABS, Q_FINAL, IALTER, Z_COMM, ZEMIBESTERR, ZABSBESTERR, ZFINALERR, TITLE_V, CENRA_V, GRATSLLOT_V, CENDEC_V, APPRA_V, APPDEC_V, ACTMJD_V, CONMJD_V, PROGID_V, LABEL_V, OBSID_V, RUN_V, EXP_V, NCOMB_V, GRATID_V, GRATSET_V, GRATBLAZ_V, SOURCE_V, FOCUS_V, TFOCUS_V, GAIN_V, NOISE_V, CCD_V, UTDATE_V, UTSTRT_V, MJDOBS_V, NAME_V, THPUT_V, RA_V, DEC_V, X_V, Y_V, XERR_V, YERR_V, THETA_V, FIBRE_V, PIVOT_V, RECMAG_V, PID_V, FRAMENAME, AXISSTART_V, AXISEND_V, MATCHSPECID, Z_INITIAL†, Z_HELIO_INITIAL†, Z_UPDATE_FLAG†, Z_UPDATE_COMM†, SLIT_VANE_CORR†, QUALITY_INITIAL, XTALKFLAG†, XTALKSCORE†, XTALKVELOFF†, XTALKCOMM†, QUALITY_UPDATE_COMM, DEPRECATED†, REVTEMPLATE†, REVCOMMENT†, Z_COMM_INITIAL†
TWOMASS	<i>JHK</i> 2MASS input catalogues	1 (<i>K</i>), 3 (<i>H</i>), 4 (<i>J</i>)	OBJID, CATNAME, TARGETNAME, TARGETID, RA, DEC, PRIORITY, MAG_1, PROGID, MAG_2, J_M_K20FE, H_M_K20FE, K_M_K20FE, RADIUS, A_B, MUK20FE, CORR, J, H, KEXT, K, KEXT_K, PREVCATNAME†, RTOT†, JTOT†, HTOT†, KTOT†
SUPERCOS	$b_J r_F$ SuperCOSMOS input catalogues	8 (b_J), 7 (r_F)	OBJID, CATNAME, TARGETNAME, TARGETID, RA, DEC, PRIORITY, MAG_1 (old b_J), PROGID, MAG_2 (old r_F), COMMENT
FSC	IRAS Faint Source Catalogue sources	126	OBJID, CATNAME, TARGETNAME, TARGETID, RA, DEC, PRIORITY, MAG_1, PROGID, MAG_2, COMMENT
RASS	ROSAT All-Sky Survey candidate AGN	113	OBJID, CATNAME, TARGETNAME, TARGETID, RA, DEC, PRIORITY, MAG_1, PROGID, MAG_2, COMMENT
HIPASS	sources from the HIPASS HI survey	119	OBJID, CATNAME, TARGETNAME, TARGETID, RA, DEC, PRIORITY, MAG_1, PROGID, MAG_2
DURUKST	Durham/UKST galaxy survey extension	78	OBJID, CATNAME, TARGETNAME, TARGETID, RA, DEC, PRIORITY, MAG_1, PROGID, MAG_2
SHAPLEY	Shapley supercluster galaxies	90	OBJID, CATNAME, TARGETNAME, TARGETID, RA, DEC, PRIORITY, MAG_1, PROGID, MAG_2
DENISI	DENIS survey galaxies, $I < 14.85$	6	OBJID, CATNAME, TARGETNAME, TARGETID, RA, DEC, PRIORITY, MAG_1, PROGID, MAG_2, COMMENT
DENISJ	DENIS survey galaxies, $J < 13.85$	5	OBJID, CATNAME, TARGETNAME, TARGETID, RA, DEC, PRIORITY, MAG_1, PROGID, MAG_2, COMMENT
AGN2MASS	2MASS red AGN survey candidates	116	OBJID, CATNAME, TARGETNAME, TARGETID, RA, DEC, PRIORITY, MAG_1, PROGID, MAG_2, MAG_3
HES	Hamburg/ESO survey candidate QSOs	129	OBJID, CATNAME, TARGETNAME, TARGETID, RA, DEC, PRIORITY, MAG_1, PROGID, MAG_2
NVSS	candidate QSOs from NVSS	130	OBJID, CATNAME, TARGETNAME, TARGETID, RA, DEC, PRIORITY, MAG_1, PROGID, MAG_2
SUMSS	bright radio sources from SUMSS	125	OBJID, CATNAME, TARGETNAME, TARGETID, RA, DEC, PRIORITY, MAG_1, PROGID, MAG_2

† New parameters created for the final data release.

SLANTED FONT V-spectrum parameters (*_V*) have matching R-spectrum (*_R*) parameters.

(iii) **Revised SuperCOSMOS Photometry:** As discussed in Jones et al. (2005) for DR2, the SuperCOSMOS magnitudes were also revised between 2001 and 2004. As was the case for DR2, **BMAG** and **RMAG** are the revised $b_J r_F$ magnitudes, which should be used for science purposes. However, some of the values in **BMAG** and **RMAG** have changed because of an improvement in the algorithm

we have used to match 6dFGS objects with new SuperCOSMOS magnitudes. This has removed much more of the deblending discussed in Sec. 2.3 of Jones et al. (2005). The historical $b_J r_F$ magnitudes held in **BMAGSEL**, **RMAGSEL** (in the **TARGET** table) and **MAG_1**, **MAG_2** (in the **SUPERCOS** table) retain their DR2 definitions and values.

Table 6. Descriptions of some key parameters in the 6dFGS database.

Parameter	Associated Table(s)	Notes
TARGETID	all	Unique source ID (integer), used to link tables.
TARGETNAME	all	Source name, ‘g##### - #####’. (Sources observed but not in the original target list have the form ‘c##### - #####’).
PROGID	all	Programme ID (integer), identifying the origin of targets. $\text{PROGID} \leq 8$ for main samples.
OBJID	all except TARGET and SPECTRA	Unique object ID (integer), assigned to each object in all input catalogues.
BMAG, RMAG	TARGET	New b_{JrF} SuperCOSMOS magnitudes following the revision for 2dFGRS by Peacock, Hambly and Read. First introduced for DR2. The most reliable b_{JrF} 6dFGS magnitudes.
ZCATVEL, ZCATERR	TARGET	Existing redshifts and errors (km s^{-1}) from ZCAT (Huchra et al. 1992) where available.
ZCATREF	TARGET	Code indicating source of ZCAT redshift: ‘126x’ for earlier 6dFGS redshifts (subsequently ingested by ZCAT), ‘392x’ for ZCAT-ingested 2dFGRS redshifts. The ‘x’ in both cases holds redshift quality (see QUALITY below). $\text{ZCATREF} \leq 99$ for other ZCAT surveys.
BMAGSEL, RMAGSEL	TARGET	Old b_{JrF} SuperCOSMOS magnitudes compiled by W. Saunders. Never used for selection and not intended for science. Previously under BMAG and RMAG in pre-DR2 releases.
TEMPLATECODE	TARGET	Code indicating cross-correlation template: ‘N’ = no redshift, ‘Z’ = ZCAT redshift (no template used), ‘T’ = 2dFGRS (no template used), 1 ... 9 = 6dFGS template code.
SPECID	SPECTRA	Unique spectral ID (integer). Different for repeat observations of the same object.
Z_ORIGIN	SPECTRA	Is ‘C’ for most spectra, which come from (c)ombined (spliced) V and R spectral frames. Is ‘V’ or ‘R’ for unpaired (orphan) data, as applicable.
KBESTR	SPECTRA	Template spectrum ID (integer) used for redshift cross-correlation.
Z_HELIO	SPECTRA	Heliocentric redshift. Corrected by -40 km s^{-1} for template offset if KBESTR = 1 or 7. The redshift intended for science use.
Z	SPECTRA	Raw measured redshift. Not intended for science use. Also template offset corrected.
Z_INITIAL †	SPECTRA	Initial copy of redshift Z, uncorrected (e.g. for slit vane shifts). Not for scientific use.
Z_UPDATE_FLAG †	SPECTRA	Z_HELIO corrections: ‘1’ if slit-vane corrected, ‘2’ if template corrected, ‘3’ for both.
Z_HELIO_INITIAL †	SPECTRA	Initial version of Z_HELIO, uncorrected (e.g. for slit vane shifts). Not for science use.
QUALITY	SPECTRA	Redshift quality, Q (integer): ‘1’ for unusable measurements, ‘2’ for possible but unlikely redshifts, ‘3’ for a reliable redshift, ‘4’ for high-quality redshifts, and ‘6’ for confirmed Galactic sources. Only $\text{QUALITY} = 3$ or 4 should be used for science. (QUALITY does <i>not</i> measure spectral quality.)
Q_FINAL	SPECTRA	Final redshift quality assigned by software. Not intended for general use. Use QUALITY.
QUALITY_INITIAL †	SPECTRA	Quality value at initial ingest, before database revision. Not for general use.
QUALITY_UPDATE_COMM †	SPECTRA	Explanation of quality value changes during database revision.
TITLE_V, TITLE_R	SPECTRA	Observation title from SDS configuration file (consisting of field name and plate number).
XTALKFLAG †	SPECTRA	Fibre number of a nearby object suspected of spectral cross-talk contamination. ‘-1’ if object is a contaminator itself. ‘0’ if neither a contaminator nor contaminee.
XTALKSCORE †	SPECTRA	Score from ‘0’ (none) to ‘5’ (high) assessing the likelihood of spectral cross-contamination.
XTALKVELOFF †	SPECTRA	Velocity offset (km s^{-1}) between contaminator and contaminee in cross-contamination.
XTALKCOMM †	SPECTRA	Comment about cross-talk likelihood.
SLIT_VANE_CORR †	SPECTRA	Correction (km s^{-1}) made to a redshift affected by slit vane shifts during observing.
REVTEMPLATE †	SPECTRA	Code of any spectral template used during the database revision of redshifts.
REVCOMMENT †	SPECTRA	Explanation of any redshift changes resulting from the database revision.
CATNAME	TWOMASS	2MASS name. (Prior to this release, CATNAME held the old names now in PREVCATNAME).
PREVCATNAME †	TWOMASS	Old 2MASS name (as at 2001).
RTOT †	TWOMASS	2MASS XSC extrapolated/total radius (2MASS <code>r_ext</code> parameter).
JTOT, HTOT, KTOT †	TWOMASS	Revised 2MASS XSC total <i>JHK</i> magnitudes (2MASS <code>j_m_ext</code> , <i>etc.</i>). For science use.
MAG_1, MAG_2	TWOMASS	Input catalogue magnitudes. Not used in TWOMASS table and so default non-value is 99.99. Superseded by JTOT, HTOT, and KTOT.
CORR	TWOMASS	Magnitude correction (based on average surface brightness) used to calculate KEXT_K.
J, H, K	TWOMASS	Old 2MASS XSC total <i>JHK</i> magnitudes. <i>JH</i> used for selection. Superseded by JTOT, <i>etc.</i>
KEXT	TWOMASS	Redundant 2MASS extrapolated <i>K</i> magnitudes, previously used to obtain KEXT_K.
KEXT_K	TWOMASS	Old total <i>K</i> magnitude estimated from KEXT and CORR. Used in original 6dFGS <i>K</i> -band selection (see Jones et al. (2004) for a discussion). Now redundant.
MAG_1, MAG_2	SUPERCOS	Old b_{JrF} SuperCOSMOS magnitudes compiled by Saunders, Parker and Read for target selection. Now superseded by the revised magnitudes BMAG and RMAG in the TARGET table.

† New parameters created for the final data release.

(iv) **Redshift Completeness:** The 2MASS and SuperCOSMOS magnitude revisions have imparted a small but non-negligible scatter between the old and new versions of $b_J r_F JHK$, particularly $b_J r_F K$. They have a non-negligible impact on estimates of 6dFGS redshift completeness at the faint end (faintest ~ 0.5 mag) of each distribution. In this regime, the new magnitudes cause increasing numbers of original 6dFGS targets to lie beyond the cut-off and increasing numbers of sources that were not original targets to fall inside the cut-off. Consequently, new target lists were compiled using the revised magnitudes, the completeness estimates were recalculated, and the results are presented along with the luminosity and mass functions in Jones et al. (in prep.).

(v) **Fibre Cross-talk:** Instances of fibre cross-talk, in which bright spectral features from one spectrum overlap with an adjacent one, have been reviewed and are now flagged in the database through three new parameters: `XTALKFLAG`, `XTALKSCORE`, and `XTALKVELOFF`, defined in Table 6. The flags are not definitive and are only meant to reflect the *likelihood* that a redshift has been affected thus. Specifically, users are urged to use extreme caution with redshifts from sources having `XTALKFLAG` ≥ 1 , `XTALKVELOFF` > 0 and `XTALKSCORE` ≥ 4 . Cases of `XTALKSCORE` = 3 are weak candidates where cross-talk is possible but not fully convincing (e.g. only the V or the R spectra are affected, but not both). `XTALKSCORE` = 4 are good candidates, but which carry the previous caveat. `XTALKSCORE` = 5 are likely cross-talk pairs which are usually confirmed through visual inspection of the spectra. Cross-talk is an uncommon occurrence (about ~ 1 percent of all spectra), and it only affects the redshifts for spectra with fewer real features than false ones. An algorithm was used to search for coincident emission lines in adjacent spectra and a cross-talk severity value assigned from 1 to 5. Users are urged to exercise caution with spectra and redshifts having cross-talk values of 3 or greater. A detailed discussion of the cross-talk phenomenon can be found in the database documentation on the website.

(vi) **Highest Redshift Sources:** Very occasionally, spurious features due to cross-talk or poor sky-subtraction led to erroneously high redshifts. This is particularly the case with the Additional Target samples (`PROGID` > 8), whose selection criteria do not necessarily ensure reliable detections at the optical wavelengths of 6dFGS spectra. Special care should be taken with the high redshift sources reported for these targets. All sources (across all programmes) with $z \geq 1.0$ were re-examined and re-classified where necessary. In addition, those sources from the primary and secondary samples (`PROGID` ≤ 8) with redshifts in the range $0.2 \leq z < 1.0$ were re-examined. There are 318 6dFGS sources with $z > 1$, mostly QSOs, and a further 7 possible cases. The highest of these is the $z = 3.793$ QSO g2037567–243832. Other notable examples are the candidate double QSO sources g0114547–181903 ($z = 2.524$) shown in Fig. 5(b) and g2052000–500523 ($z = 1.036$). Deep follow-up imaging in search of a foreground source is necessary to decide whether these sources are individual gravitationally lensed QSOs or genuine QSO pairs. Even with such data in hand, the distinction is quite often equivocal

(e.g. Faure et al. 2003; Hennawi et al. 2006, and references therein).

(vii) **Orphan Fields:** The final data release includes (for the first time) data from 29 orphan fields. These are fields that, for various reasons, are missing either the V or R half of the spectrum. These fields have a reduced redshift yield because of the restricted access to redshifted spectral features, particularly in the case of missing R spectra. Orphan field data are flagged in the database through the `Z_ORIGIN` parameter (see Table 6).

(viii) **Re-examination of Q=1 and Q=2 spectra:** All sources originally classified as either being extragalactic and $Q = 2$, or non-2MASS-selected (`PROGID` > 4) and $Q = 1$, have been re-examined. This was done primarily to improve the identification of faint high-redshift QSOs. Many QSOs were poorly identified in the early stages of the survey due to the absence of suitable QSO templates for redshifting. Redshift data for 4506 $Q = 2$ and 3687 $Q = 1$ sources were checked, and the database updated where necessary.

(ix) **Image Examination of all Q=6 Sources and Re-redshifting:** In the initial redshifting effort, 6212 sources were classified as $Q = 6$ (i.e. confirmed Galactic sources with $z = 0$) on the basis of their spectra and redshifts alone. Once spectral and imaging data were assembled side-by-side in the 6dFGS database, it was straightforward to examine the postage-stamp images of these sources, given their spectral classification. Most were confirmed as being true Galactic sources (stars, HII regions, planetary nebulae, YSOs), or Galactic objects in close proximity to an extragalactic source. A small number were also found to be 2MASS imaging artefacts, or parts of larger objects. However, a significant number (847) were found to be galaxies with near-zero redshifts, which were subsequently re-redshifted and re-classified, and updated in the database. In some cases, even though the source was clearly a galaxy on the basis of its imaging, its true redshift could not be obtained. The most common causes were scattered light from a nearby star, or contamination from a foreground screen of Galactic emission.

(x) **Anomalous K-z Sources with Q=3,4:** The $K-z$ magnitude-redshift relation was used to identify anomalous redshifts ($Q = 3, 4$) outside the envelope normally spanned by this relation at typical 6dFGS redshifts. The postage-stamp images of these sources were compared to their spectra and redshifts to decide if the initial redshift was incorrect. There were 120 objects deemed to have an anomalous $K-z$; 94 were found to have incorrect redshifts, which were re-examined and re-incorporated into the database.

(xi) **Correction of Slit-Vane Shifted Fields:** Midway through the survey it became apparent that the magnetically-held vane supporting the spectrograph slit was shifting occasionally between exposures. This problem was discovered prior to DR2 but the affected redshifts were withheld; they have been corrected and provided in the final release. The resulting spectra from affected fields show a small wavelength offset (greater than $\pm 0.75\text{\AA}$ and up to a few \AA), dependent on fibre number. The V and R spectral halves were sometimes affected individually, and at other times in unison. Instances of shifting were isolated by comparing the wavelength of the $[\text{OI}]\lambda 5577.4\text{\AA}$

sky line, as measured from the 6dFGS spectra, to its true value. A search found 125 affected fields able to be satisfactorily fit (measured [OI] against fibre number) and redshift corrected. In all, 18 438 galaxies were corrected in this way (approximately 14 percent of the entire sample of *all* spectra), with corrections $\lesssim 12\text{\AA}$. Redshift template values **KBESTR** were used to determine whether to apply a correction. If an object used **KBESTR** = 1, 2 (corresponding to early-type galaxy templates), the redshift was deemed to be due to absorption-lines, which occur predominantly in the V half. If the corresponding V frame was indeed slit-vane affected, a correction was applied to the redshift for this galaxy based on the fit to the V frame *alone*. Alternatively, if **KBESTR** = 3, 4, 5 (corresponding to late-type galaxy templates), then the redshift was deemed to be emission-line dependent, and the corresponding R frame correction was made where necessary. Users can find those galaxies with slit-vane corrected redshifts through the new **SLITVANECORR** parameter, which gives the size (in km s^{-1}) of any corrections applied. Unaffected galaxies have **SLITVANECORR** = 0. The corrected redshifts are the heliocentric redshifts held by **Z_HELIO**.

(xii) **Correction for Template Offset Values:** Various tests comparing 6dFGS redshifts to independent measurements found small systematic offsets in the case of a couple of templates. The discrepancy is almost certainly due to a zero-point error in the velocity calibration of the template spectra. This effect was discovered prior to DR2 and is discussed in Jones et al. (2005), although no corrections were applied to the affected redshifts in that release. For this final release, corrections of -40 km s^{-1} have been applied to redshifts derived from templates **KBESTR** = 1, 7. The corrected redshifts are both the raw (**Z**) and heliocentric (**Z_HELIO**) redshifts. The redshift offsets were found to be consistent between a 2004 comparison of 16 127 6dFGS and ZCAT redshifts, and a 2007 comparison of 443 redshifts from various peculiar velocity surveys (Bernardi et al. 2003; Smith et al. 2000, 2004; Wegner et al. 2003).

(xiii) **Telluric Sky Line Subtraction:** The redshifting software used by 6dFGS automatically removed telluric absorption lines from spectra, but the database spectra have hitherto retained their imprint. For the final release we have re-spliced spectra and incorporated telluric line removal. An example spectrum is shown in Fig. 5. A small number of spectra which failed to re-splice successfully have had their old telluric-affected versions retained.

(xiv) **Spurious Clustering:** The entire sample of reliable redshifts ($Q = 3, 4$) was tested for spurious clusters, caused by any systematic effect that produces noticeable numbers of objects from the same field with nearly identical redshifts. Possible causes include poor sky subtraction and/or splicing of spectra, and the fibre cross-talk effect discussed in item (v). Fields containing at least 16 cases of galaxy groups (3 or more members) with redshift differences of less than 30 km s^{-1} had their redshifts re-examined: 171 galaxies from 7 fields. No prior knowledge of real galaxy clustering was used for the re-redshifting, and the database was updated with new redshifts and quality assignments. The field 0058m30 was particularly prominent with 48 galaxies at or near an apparent red-

shift of 0.1590. This was due to the over-subtraction and subsequent mis-identification of the 7600\AA telluric absorption band with redshifted $\text{H}\alpha$. A further 134 objects with redshifts in the range $0.1585 \leq z \leq 0.1595$ were re-examined for this effect, and 118 given corrected z or Q values. Almost all of the affected spectra are among the earliest observations of survey data (2001), prior to the switch to VPH gratings.

(xv) **RASS sources:** All sources in the ROSAT All-Sky Survey (RASS) Additional Target sample (**PROGID** = 113; 1850 sources) were re-examined using the full QSO template set. The database was updated with new redshifts and quality assignments. Mahoney et al. (2009) describe the selection and characteristics of this sample in more detail.

4 SOUTHERN LARGE-SCALE STRUCTURES

4.1 Sky projections

The wide sky coverage of the 6dF Galaxy Survey affords the most detailed view yet of southern large-scale structures out to $cz \sim 30\,000 \text{ km s}^{-1}$. The 6dFGS extends the sky coverage of the 2dFGRS (Colless et al. 2001) by an order of magnitude, and likewise improves by an order of magnitude on the sampling density of the all-sky PSCz survey (Branchini et al. 1999; Saunders et al. 2000). Prominent southern structures such as Shapley, Hydra-Centaurus and Horologium-Reticulum have received much special attention in their own right over recent years (Raychaudhury 1989; Quintana et al. 1995; Drinkwater et al. 1999; Reisenegger et al. 2000; Bardelli et al. 2000; Kaldare et al. 2003; Woudt et al. 2004; Fleenor et al. 2005, 2006; Radburn-Smith et al. 2006; Proust et al. 2006). However, a detailed large-scale mapping of all intervening structures (and the voids between them) with a purpose-built instrument has remained unavailable until now. The complementary 2MASS Redshift Survey (2MRS; Huchra et al., in prep) uses the 6dFGS in the south to provide an all-sky redshift survey of some 23 000 galaxies to $K = 11.25$ ($\bar{z} = 0.02$). It is hoped it will one day be extended to reach an equivalent depth to 6dFGS in the north in those areas not already covered by SDSS.

Figures 6 and 7 show the $z < 0.2$ universe as seen by 6dFGS in the plane of the sky, projected in Galactic coordinates. The two figures show the northern and southern Galactic hemispheres, respectively. Familiar large-scale concentrations such as Shapley are obvious, and several of the key structures have been labelled. At $z < 0.02$, filamentary structures such as the Centaurus, Fornax and Sculptor walls (Fairall 1998) interconnect their namesake clusters in a manner typical of large structures generally. At $z \approx 0.006$ to 0.01 the Centaurus wall crosses the Galactic plane Zone of Avoidance (ZoA) and meets the Hydra wall at the Centaurus cluster. The Hydra wall then extends roughly parallel to the ZoA before separating into two distinct filaments at the adjacent Hydra/Antlia clusters, both of which extend into the ZoA. Behind these, at $z = 0.01$ to 0.02, a separate filament incorporates the

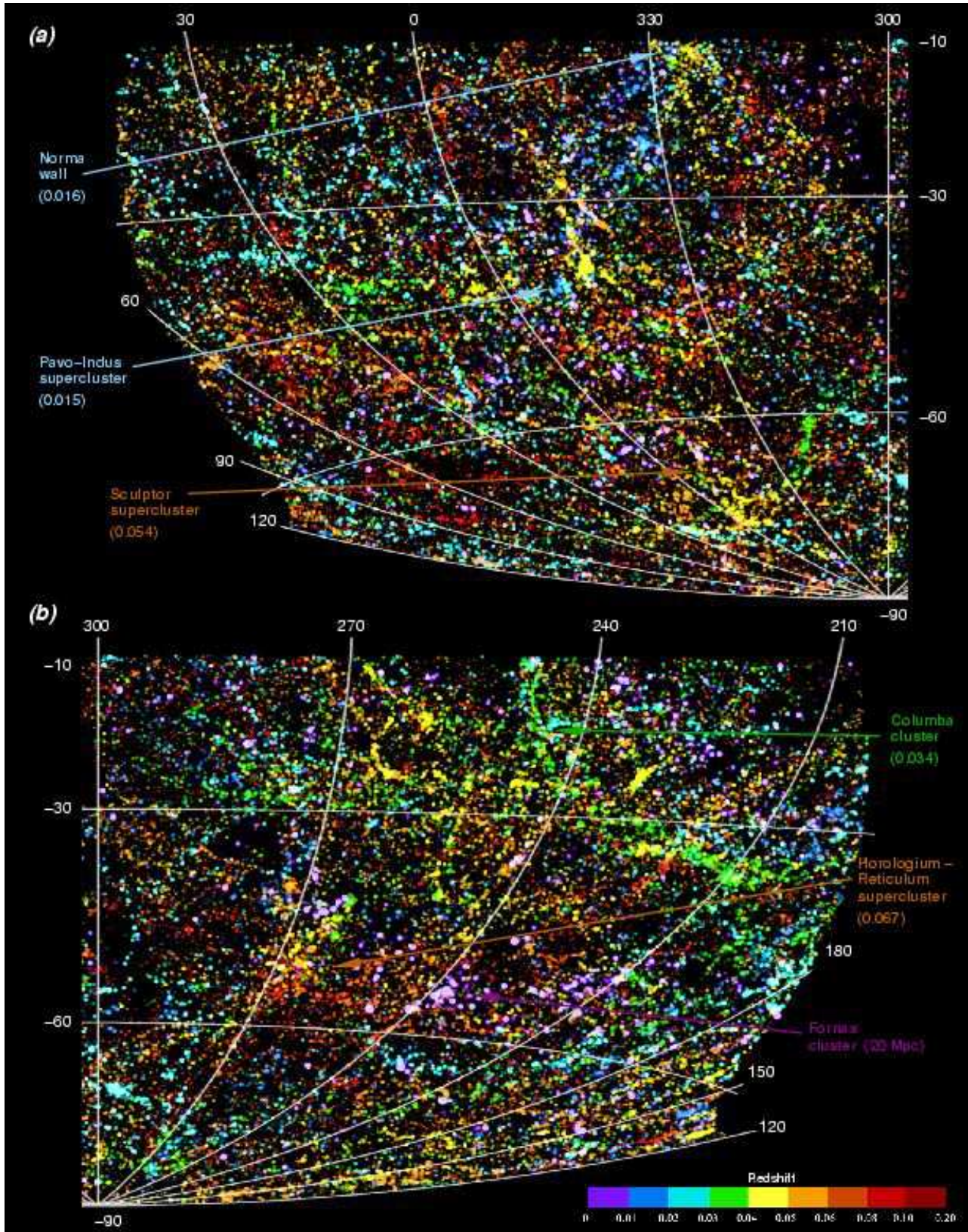


Figure 6. The distribution of galaxies in the 6dFGS shown in an Aitoff projection of Galactic coordinates across the southern Galactic hemisphere; redshifts are colour-coded from blue (low, $z < 0.02$) to red (high, $z > 0.1$). Some of the major large-scale structures are labelled.

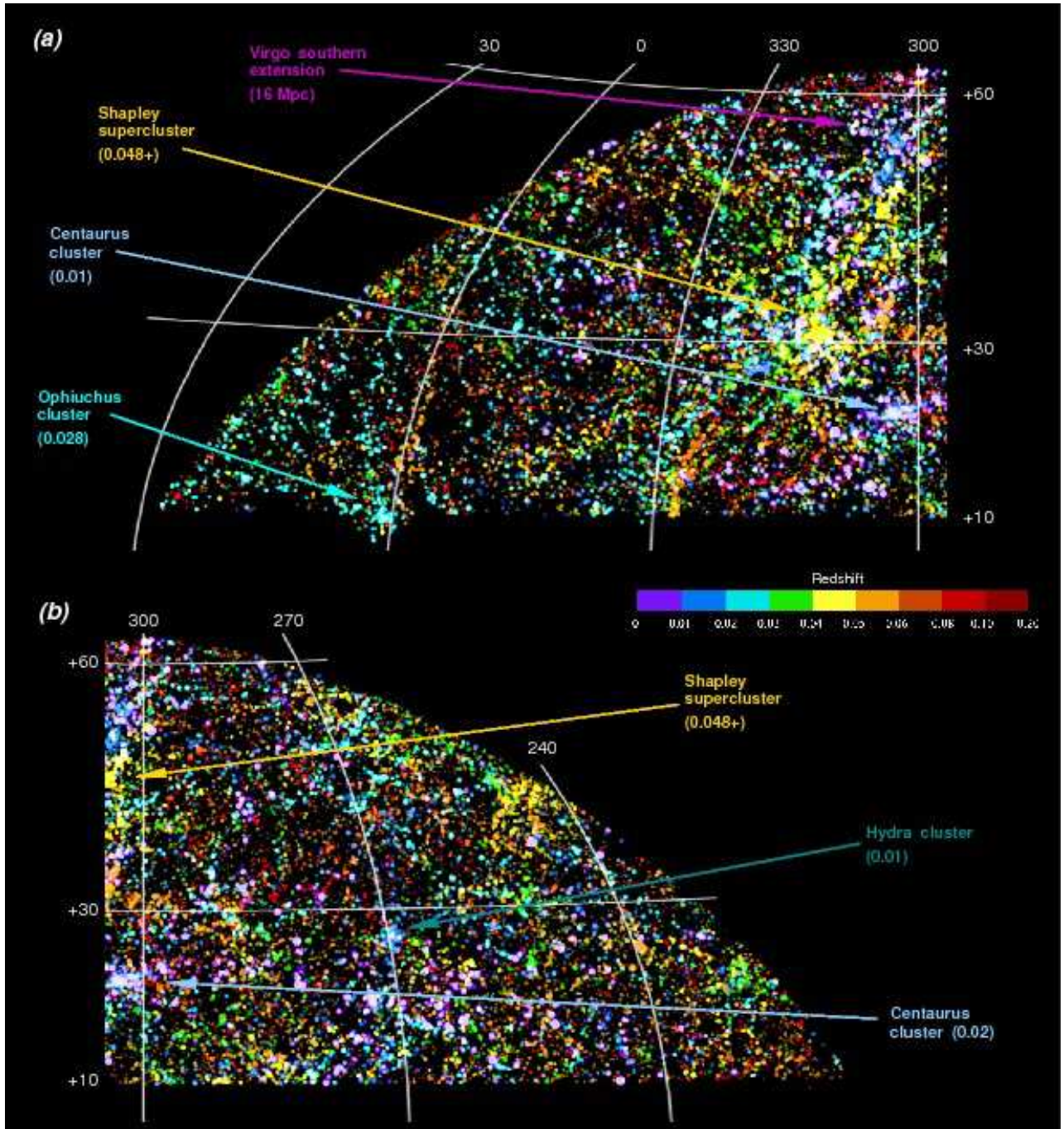


Figure 7. Same as Fig. 6 except showing the northern Galactic hemisphere.

Norma and Centaurus-Crux clusters, and encompasses the putative Great Attractor region (Woudt et al. 2004; Radburn-Smith et al. 2006, and references therein). Beyond these, at $z = 0.04$ to 0.05 , lies the Shapley Supercluster complex, a massive concentration of clusters thought to be responsible for 10 percent of the Local Group motion (Raychaudhury 1989; Reisenegger et al. 2000; Bardelli et al. 2000) or even more (Quintana et al. 1995; Drinkwater et al. 1999; Proust et al. 2006).

4.2 Declination slice projections

Figures 8 and 9 show an alternative projection of these structures, as conventional radial redshift maps, cross-sectioned in declination. The two figures show the same data on two different scales, out to limiting redshifts of $z = 0.05$ and 0.1 respectively. The empty sectors in our maps correspond to the ZoA region. These declination-slice sky views can also be cross-referenced with the Aitoff-projected sky redshift maps presented in Jones et al. (2005) for the 6dFGS data available up to 2004, as well as Figs 6 and 7.

Figure 9 similarly displays the local universe out to $z = 0.1$ with hitherto unseen detail and sky coverage. While it extends and confirms the now familiar labyrinth of filaments and voids, it also reveals evidence of inhomogeneity on a still larger scale — the plot for $-40^\circ < \delta < -30^\circ$ (middle right panel) is a good example. A large under-dense region ($\Delta z \sim 0.05$) at $\alpha \approx 4$ hr to 5 hr separates regions of compact high-density filaments; similar inhomogeneities are visible in the other plots. An extraordinarily large void ($\Delta z = 0.03$ by 0.07) is apparent in the plot for $-20^\circ < \delta < -10^\circ$, towards $\alpha \approx 23$ hr. Other voids of this size are apparent when the data are examined in Cartesian coordinates. The most extreme inhomogeneity, however, is the over-dense Shapley region, which is unique within the sample volume.

Erdogdu et al. (2006a) have used spherical harmonics and Wiener filtering to decompose the density and velocity field of the shallower 2MRS. The correspondence between the largest-scale superclusters and voids seen in both surveys at $z < 0.05$ is clear. Our southernmost projection ($-90^\circ < \delta < -60^\circ$) confirms the most distant (Pavo) of the three tentative superclusters of Fairall & Woudt (2006) while indicating that the other two are not major overdensities. We point out that this southern region is where 6dFGS coverage is generally lowest, with below-average completeness between 0 hr and 6 hr and around the pole (poor sky coverage), and at 11 hr to 17 hr (ZoA). Azimuthal stretching effects are also evident, due to the wide R.A. span of single fields at polar declinations.

Work is currently underway cataloguing new clusters and groups from 6dFGS (Merson et al, in prep.) using a percolation-inferred friends-of-friends algorithm (Huchra & Geller 1982; Eke et al. 2004). At the same time, a preliminary list of ~ 500 void regions has been compiled as a reference for future work on under-dense regions. A power spectrum analysis of the clustering of 6dFGS galaxies will be published elsewhere.

5 CONCLUSION

The 6dF Galaxy Survey (6dFGS) is a combined redshift and peculiar velocity survey over most of the southern sky. Here we present the final redshift catalogue for the survey (version 1.0), consisting of 125 071 extragalactic redshifts over the whole southern sky with $|b| > 10^\circ$. Of these, 110 256 are new redshifts from 136 304 spectra obtained with the United Kingdom Schmidt Telescope (UKST) between 2001 May and 2006 January. With a median redshift of $z_{1/2} = 0.053$, 6dFGS is the deepest hemispheric redshift survey to date. Redshifts and associated spectra are available through a fully-searchable online SQL database, interlinked with photometric and imaging data from the 2MASS XSC, SuperCOSMOS and a dozen other input catalogues. Peculiar velocities and distances for the brightest 10 percent of the sample will be made available in a separate future release.

In this paper we have mapped the large-scale structures of the local ($z < 0.1$) southern universe in unprecedented detail. In addition to encompassing well-known superclusters such as Shapley and Hydra-Centaurus,

the 6dFGS data reveal a wealth of new intervening structures. The greater depth and sampling density of 6dFGS compared to earlier surveys of equivalent sky coverage has confirmed hundreds of voids and furnished first redshifts for around 400 southern Abell clusters (Abell, Corwin & Olowin 1989). More detailed quantitative analyses of 6dFGS large-scale structure will be the subject of future publications.

The unprecedented combination of angular coverage and depth in 6dFGS offers the best chance yet to minimise systematics in the determination of the luminosity and stellar mass functions of low-redshift galaxies, both in the near-infrared and optical (e.g. Jones et al. 2006). While surveys containing $\sim 10^5$ -galaxy redshifts (such as 6dFGS) have now reduced random errors to comparable levels of high precision, systematic errors remain the dominant source of the differences between surveys. For example, the evolutionary corrections that initially beset comparisons between 2dFGRS and SDSS (cf. Norberg et al. 2002; Blanton et al. 2001) are negligible for 6dFGS, which spans lookback times of only 0.2 to 0.7 Gyr across $[0.5\bar{z}, 1.5\bar{z}]$ (compared to 0.5 to 1.3 Gyr for SDSS and 2dFGRS). The minimisation of such systematics are a feature of the 6dFGS stellar mass and luminosity functions derived for the final redshift set (Jones et al., in prep).

In addition to these studies, 6dFGS redshift data have already been used to support a variety of extragalactic samples selected from across the electromagnetic spectrum. Deep HI surveys planned for next-generation radio telescopes (Blake et al. 2004; van Driel 2005; Rawlings 2006; Johnston et al. 2008) will also benefit from this redshift information as they probe the gas content of the local southern universe over comparable volumes.

ACKNOWLEDGEMENTS

DHJ acknowledges support from Australian Research Council Discovery–Projects Grant (DP-0208876), administered by the Australian National University. JPH acknowledges support from the US National Science Foundation under grant AST0406906.

We dedicate this paper to two colleagues who made important contributions to the 6dF Galaxy Survey before their passing: John Dawe (1942 – 2004), observer and long-time proponent of wide-field fibre spectroscopy on the UKST from its earliest days, and Tony Fairall (1943 – 2008), whose unique insights from a career-long dedication to mapping the southern universe underpin much of the interpretation contained herein.

REFERENCES

- Abell, G. O., Corwin, Jr., H. G., Olowin, R. P., 1989, *ApJS*, 70, 1
- Abazajian, K., et al., (the SDSS Collaboration) 2009, submitted, (astro-ph/0812.0649)
- Andernach, H., Tago, E., Einasto, M., Einasto, J., Jaaniste, J., 2005, in *Nearby Large-Scale Structures and the Zone of Avoidance*, *Astronomical Society of*

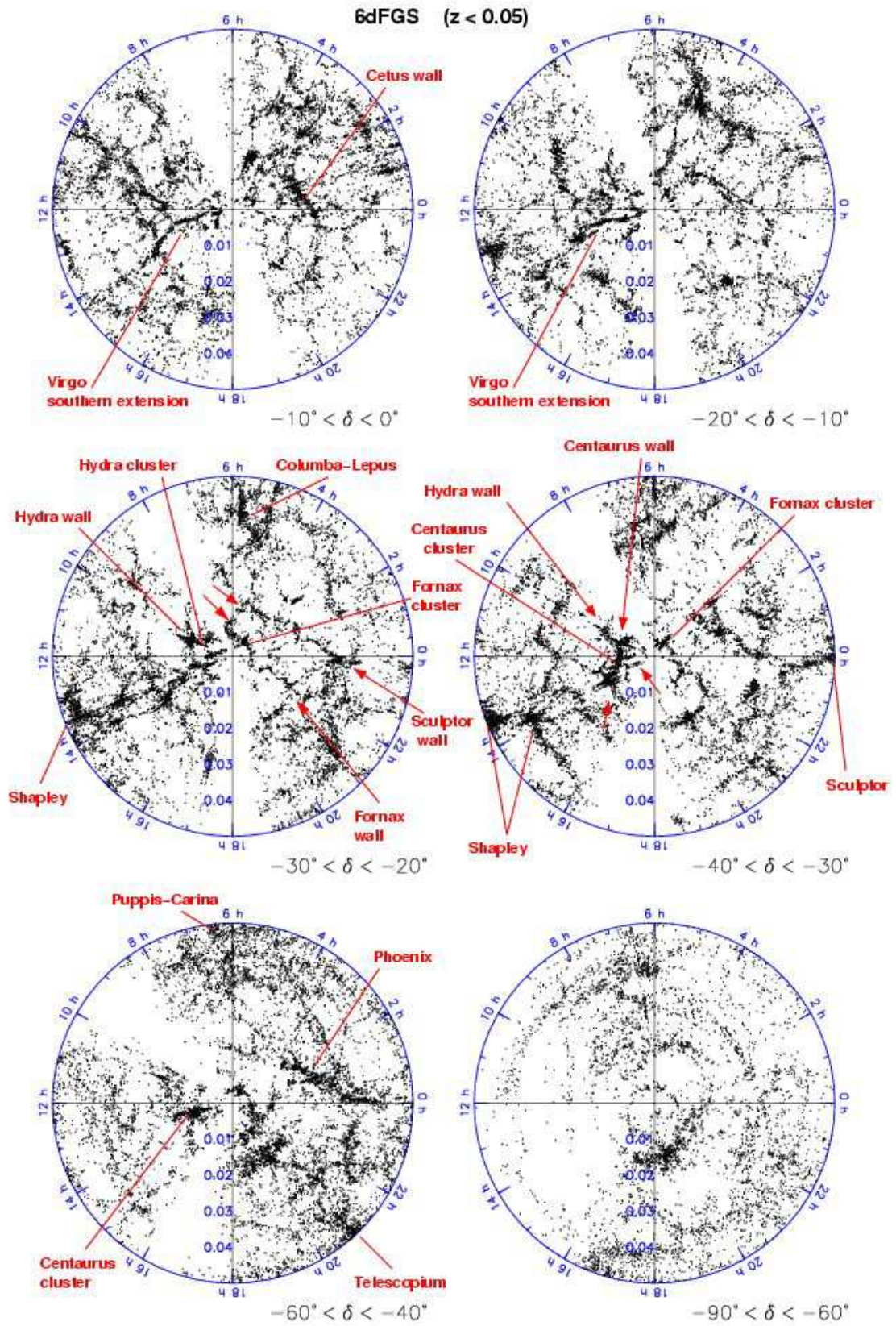


Figure 8. 6dFGS redshift maps out to $z = 0.05$, in declination slices of varying width from the equator to the pole.

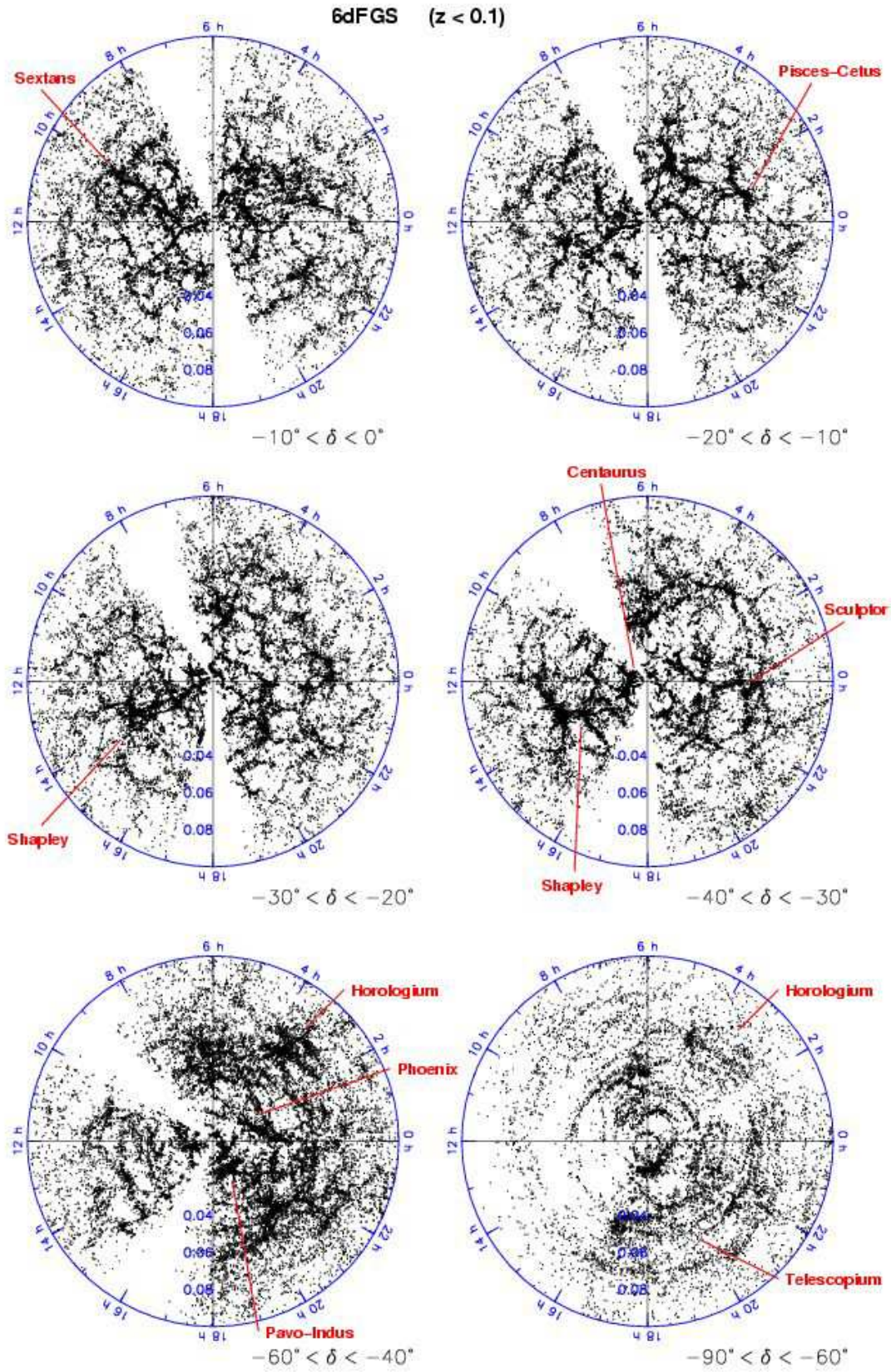


Figure 9. Same as Fig. 8, except on a larger scale out to $z = 0.1$.

- the Pacific Conference Series vol. 329, A. P. Fairall and P. A. Woudt eds., p283
- Bardelli, S., Zucca, E., Zamorani, G., Moscardini, L., Scaramella, R., 2000, *MNRAS*, 312, 540
- Baugh, C. M., 2006, *Reports of Progress in Physics*, 69, 3101
- Bell, E. F., de Jong, R. S., 2001, *ApJ*, 550, 212
- Bell, E. F., McIntosh, D. H., Katz, N., Weinberg, M. D., 2003, *ApJS*, 149, 289
- Bennett, C. L., Halpern, M., Hinshaw, G., Jarosik, N., Kogut, A., Limon, M., Meyer, S. S., Page, L., et al., 2003, *ApJS*, 148, 1
- Bernardi, M., et al., (SDSS team), 2003, *AJ*, 125, 1849
- Blake, C. A., Abdalla, F. B., Bridle, S. L., Rawlings, S., 2004, *New Astronomy Review*, 48, 1063
- Blanton, M. R., et al., (SDSS team), 2001, *AJ*, 121, 2358
- Boué, G., Adami, C., Durret, F., Mamon, G. A., Cayatte, V., 2008, *A&A*, 479, 335
- Branchini, E., Teodoro, L., Frenk, C. S., Schmoltdt, I., Efstathiou, G., White, S. D. M., Saunders, W., Sutherland, W., et al., 1999, *MNRAS*, 308, 1
- Burkey, D., Taylor, A. N., 2004, *MNRAS*, 347, 255
- Campbell, L., Saunders, W., Colless, M., 2004, *MNRAS*, 350, 1467
- Cole, S., et al., (2dFGRS team), 2005, *MNRAS*, 362, 505
- Colless, M. et al., (2dFGRS team), 2001, *MNRAS*, 328, 1039
- Drinkwater, M. J., Proust, D., Parker, Q. A., Quintana, H., Slezak, E., 1999, *Publications of the Astronomical Society of Australia*, 16, 113
- Eke, V. R., et al., (2dFGRS team), 2004, *MNRAS*, 348, 866
- Erdogdu, P., Lahav, O., Huchra, J. P., Colless, M., Cutri, R. M., Falco, E., George, T., Jarrett, T., et al., 2006a, *MNRAS*, 373, 45
- Erdogdu, P., Huchra, J. P., Lahav, O., Colless, M., Cutri, R. M., Falco, E., George, T., Jarrett, T., et al., 2006b, *MNRAS*, 368, 1515
- Fairall, A. P., 1998, *Large-Scale Structures in the Universe*, Wiley-Praxis, Chichester
- Fairall, A. P., Woudt, P. A., 2006, *MNRAS*, 366, 267
- Faure, C., Alloin, D., Gras, S., Courbin, F., Kneib, J.-P., Hudelot, P., 2003, *A&A*, 405, 415
- Fleenor, M. C., Rose, J. A., Christiansen, W. A., Hunstead, R. W., Johnston-Hollitt, M., Drinkwater, M. J., Saunders, W., 2005, *AJ*, 130, 957
- Fleenor, M. C., Rose, J. A., Christiansen, W. A., Johnston-Hollitt, M., Hunstead, R. W., Drinkwater, M. J., Saunders, W., 2006, *AJ*, 131, 1280
- Fluke, C. J., Barnes, D. G., Jones, N. T., 2008, *ArXiv e-prints*, in press (0810.4201)
- Hambly, N. C., MacGillivray, H. T., Read, M. A., Tritton, S. B., Thomson, E. B., Kelly, B. D., Morgan, D. H., Smith, R. E., et al., 2001a, *MNRAS*, 326, 1279
- Hambly, N. C., Davenhall, A. C., Irwin, M. J., MacGillivray, H. T., 2001b, *MNRAS*, 326, 1315
- Hennawi, J. F., Strauss, M. A., Oguri, M., Inada, N., Richards, G. T., Pindor, B., Schneider, D. P., Becker, R. H., et al., 2006, *AJ*, 131, 1
- Huchra, J. P., Geller, M. J., 1982, *ApJ*, 257, 423
- Huchra, J. P., Geller, M., Clemens, C., Tokarz, S., Michel, A., The Center for Astrophysics Redshift catalog, *Bull. C. D. S.*, 41, 31
- Jarrett, T. H., Chester, T., Cutri, R., Schneider, S., Rosenberg, J., Huchra, J. P., Mader, J., 2000, *AJ*, 120, 298
- Johnston, S., Taylor, R., Bailes, M., Bartel, N., Baugh, C., Bietenholz, M., Blake, C., Braun, R., et al., 2008, *Experimental Astronomy*, 22, 151
- Jones, D. H., Saunders, W., Colless, M., Read, M. A., Parker, Q. A., Watson, F. G., Campbell, L. A., Burkey, D., et al., 2004, *MNRAS*, 355, 747
- Jones, D. H., Saunders, W., Read, M., Colless, M., 2005, *PASA*, 22, 277
- Jones, D. H., Peterson, B. A., Colless, M., Saunders, W., 2006, *MNRAS*, 369, 25
- Kaldare, R., Colless, M., Raychaudhury, S., Peterson, B. A., 2003, *MNRAS*, 339, 652
- Mauch, T., Sadler, E. M., 2007, *MNRAS*, 375, 931
- Mahoney, E. K., Croom, S. M., Boyle, B. J., Edge, A. C., Sadler, E. M., 2009, *MNRAS*, *subm.*
- Mauduit, J.-C., Mamon, G. A., 2007, *A&A*, 475, 169
- McIntosh, D. H., Bell, E. F., Weinberg, M. D., Katz, N., 2006, *MNRAS*, 373, 1321
- Norberg, P., et al., (2dFGRS team), 2002, *MNRAS*, 336, 907
- Parker, Q. A., Watson, F. G., Miziarski, S., 1998, in *Arribas S., Mediavilla E., Watson F., eds., ASP Conf Ser. Vol 152, Fiber Optics in Astronomy III*. *Astron. Soc. Pac.*, San Francisco, p 80
- Perlmutter, S., Aldering, G., Goldhaber, G., Knop, R. A., Nugent, P., Castro, P. G., Deustua, S., Fabbro, S., et al., 1999, *ApJ*, 517, 565
- Porter, S. C., Raychaudhury, S., 2005, *MNRAS*, 364, 1387
- Proust, D., Quintana, H., Carrasco, E. R., Reisenegger, A., Slezak, E., Muriel, H., Dünner, R., Sodr e, Jr., L., et al., 2006, *A&A*, 447, 133
- Quintana, H., Ramirez, A., Melnick, J., Raychaudhury, S., Slezak, E., 1995, *AJ*, 110, 463
- Radburn-Smith, D. J., Lucey, J. R., Woudt, P. A., Kraan-Korteweg, R. C., Watson, F. G., 2006, *MNRAS*, 369, 1131
- Rawlings, S., *The Scientific Requirements for Extremely Large Telescopes*, *Proceedings of the 232nd IAU Symposium*, P. Whitelock, M. Dennefeld and B. Leibundgut eds., Cambridge University Press, 2006, p. 86
- Raychaudhury, S., 1989, *Nature*, 342, 251
- Reisenegger, A., Quintana, H., Carrasco, E. R., Maze, J., 2000, *AJ*, 120, 523
- Riess, A. G., Filippenko, A. V., Challis, P., Clocchiatti, A., Diercks, A., Garnavich, P. M., Gilliland, R. L., Hogan, C. J., et al., 1998, *AJ*, 116, 1009
- Sadler, E. M., Cannon, R. D., Mauch, T., Hancock, P. J., Wake, D. A., Ross, N., Croom, S. M., Drinkwater, M. J., et al., 2007, *MNRAS*, 381, 211
- Saunders, W., Sutherland, W. J., Maddox, S. J., Keeble, O., Oliver, S. J., Rowan-Robinson, M., McMahon, R. G., Efstathiou, G. P., et al., 2000, *MNRAS*, 317, 55
- Schmidt, B. P., Suntzeff, N. B., Phillips, M. M., Schommer, R. A., Clocchiatti, A., Kirshner, R. P., Garnavich, P., Challis, P., et al., 1998, *ApJ*, 507, 46
- Smith, R. J., Lucey, J. R., Hudson, M. J., Schlegel, D. J.,

- Davies, R. L., 2000, MNRAS, 313, 469
- Smith, R. J., Hudson, M. J., Nelan, J. E., Moore, S. A. W., Quinney, S. J., Wegner, G. A. Davies, R. L., et al., 2004, AJ, 128, 1558
- Spergel, D. N., Bean, R., Doré, O., Nolta, M. R., Bennett, C. L., Dunkley, J., Hinshaw, G., Jarosik, N., et al., 2007, ApJS, 170, 377
- Springob, C. M., Masters, K. L., Haynes, M. P., Giovanelli, R., Marinoni, C., 2007, ApJS, 172, 599
- Stoche, J. T., Penton, S. V., Danforth, C. W., Shull, J. M., Tumlinson, J., McLin, K. M., 2006, ApJ, 641, 217
- van Driel, W., SF2A-2005 Semaine de l'Astrophysique Française, F. Casoli, T. Contini, J. M. Hameury and L. Pagani eds., Edp-Sciences Conference Series, 2005, p. 701
- Watson, F. G., Parker, Q. A., Bogatu, G., Farrell, T. J., Hingley, B. E., Miziarski, S., 2000, in Iye M., Moorwood A. F., eds., Proc. SPIE Vol. 4008, Optical and IR Telescope Instrumentation and Detectors, SPIE, Bellingham, WA, p. 123
- Wegner, G., Bernardi, M., Willmer, C. N. A., da Costa, L. N., Alonso, M. V., Pellegrini, P. S., Maia, M. A. G., Chaves, O. L., et al., 2003, AJ, 126, 2268
- Woudt, P. A., Kraan-Korteweg, R. C., Cayatte, V., Balkowski, C., Felenbok, P., 2004, A&A, 415, 9
- York, D. G., et al., (SDSS team), 2000, AJ, 120, 1579
- Zaroubi, S., Branchini, E., 2005, MNRAS, 357, 527